Identification of the N-Linked Glycosylation Sites of the Human Relaxin Receptor and Effect of Glycosylation on Receptor Function[†]

Y. Yan,[‡,§] D. J. Scott,[§,||] T. N. Wilkinson,[§,||] J. Ji,[‡] G. W. Tregear,[§,||] and R. A. D. Bathgate*[,§,||]

Department of Biochemistry and Molecular Biology, College of Life Sciences, The National Laboratory of Protein Engineering and Plant Genetic Engineering, Peking University, Beijing 100871, P. R. China, and Howard Florey Institute and Department of Biochemistry and Molecular Biology, University of Melbourne, Victoria 3010, Australia

Received March 27, 2008; Revised Manuscript Received April 28, 2008

ABSTRACT: The relaxin receptor, RXFP1, is a member of the leucine-rich repeat-containing G-protein-coupled receptor (LGR) family. These receptors are characterized by a large extracellular ectodomain containing leucine-rich repeats which contain the primary ligand binding site. RXFP1 contains six putative Asn-linked glycosylation sites in the ectodomain at positions Asn-14, Asn-105, Asn-242, Asn-250, Asn-303, and Asn-346, which are highly conserved across species. N-Linked glycosylation is the most common post-translational modification of G-protein-coupled receptors, although its role in modulating receptor function differs. We herein investigate the actual N-linked glycosylation status of RXFP1 and the functional ramifications of these post-translational modifications. Site-directed mutagenesis was utilized to generate single- or multiple-glycosylation site mutants of FLAG-tagged human RXFP1 which were then transiently expressed in HEK-293T cells. Glycosylation status was analyzed by immunoprecipitation and Western blot and receptor function analyzed with an anti-FLAG ELISA, ^{33}P-H2 relaxin competition binding, and cAMP activity measurement. All of the potential N-glycosylation sites of RXFP1 were utilized in HEK-293T cells, and importantly, disruption of glycosylation at individual or combinations of double and triple sites had little effect on relaxin binding. However, combinations of glycosylation sites were required for cell surface expression and cAMP signaling. In particular, N-glycosylation at Asn-303 of RXFP1 was required for optimal intracellular cAMP signaling. Hence, as is the case for other LGR family members, N-glycosylation is essential for the transport of the receptor to the cell surface. Additionally, it is likely that glycosylation is also essential for the conformational changes required for G-protein coupling and subsequent cAMP signaling.

Relaxin is a peptide hormone of the insulin/relaxin superfamily and like other members of this family has a characteristic two-chain structure linked by two disulfide bridges and an intrachain disulfide bond (*1*). There are three relaxin genes in humans and higher primates designated RLN1,[1] RLN2, and RLN3, whereas other mammalian species have only two relaxin genes, RLN1 and RLN3. The product of the RLN3 gene, relaxin-3, is produced in the brain and is a putative neuropeptide (*2*). The product of the human RLN2 gene, H2 relaxin, is the ortholog of the RLN1 gene in other mammalian species and is the form of relaxin used in this work. Relaxin is produced by the corpus luteum and/or placenta during pregnancy and has numerous essential actions in the reproductive tract (*3*). More recently, a growing body of evidence that relaxin has important roles in a number of nonreproductive tissues associated with pregnancy, including the heart (*4*), kidney (*5*), and brain (*6, 7*), has begun to emerge. Additionally, research has demonstrated that locally produced relaxin also has more general physiological roles, including the regulation of collagen biosynthesis in many tissues, which occurs in both males and females (*8*). This has led to clinical trials using relaxin to treat fibrotic diseases such as scleroderma (*9*).

Unlike insulin, which signals via a tyrosine kinase receptor, relaxin signals via leucine-rich repeat-containing G-protein-coupled receptor 7 (LGR7) (*10*), now known as relaxin family peptide receptor 1 (RXFP1) (*11*). Additionally, H2 relaxin can bind to and activate RXFP2 (LGR8) (*12*), the specific receptor for INSL3 (*13*). LGRs are mosaic proteins that contain an extracellular domain with multiple leucine-rich repeats (LRRs), and a GPCR 7 transmembrane domain (*14*). Among the members of the LGR family, which includes the well-characterized glycoprotein hormone receptors FSHR, LHR, and TSHR, the recognition and activation steps are carried out by separate domains of the receptors (*15*). The

[†] This work was supported by Australian National Health and Medical Research Council (NHMRC) Project Grants 30012 and 454375 to R.A.D.B. and G.W.T. and a grant from the National Key Basic Research Program of China (Grant 2006CB910103 to J.J.).

* To whom correspondence should be addressed: Howard Florey Institute, University of Melbourne, Victoria 3010, Australia. E-mail: bathgate@florey.edu.au. Phone: +61 3 8344 5648. Fax: +61 3 9348 1707.

[‡] Peking University.

[§] Howard Florey Institute, University of Melbourne.

[||] Department of Biochemistry and Molecular Biology, University of Melbourne.

[1] Abbreviations: LGR, leucine-rich repeat-containing G-protein-coupled receptor; RXFP, relaxin family peptide receptor; RLN1, relaxin-1 gene; RLN2, relaxin-2 gene; RLN3, relaxin-3 gene; H2 relaxin, human relaxin-2 peptide; TM, transmembrane; LRRs, leucine-rich repeats; INSL3, insulin-like peptide 3; LDLa, low-density lipoprotein-class A; GPCR, G-protein-coupled receptor.

10.1021/bi800535b CCC: $40.75
Published on Web 06/06/2008

LRRs of RXFP1 and RXFP2 are the sites of primary ligand binding (*12, 16, 17*), and there is an additional binding site in the transmembrane exoloops (*18*). RXFP1 and RXFP2 are members of LGR subfamily C due to their unique LDL-class A (LDLa) modules at the N-termini of the receptors which are essential for ligand-stimulated intracellular cAMP signaling (*19, 20*).

Glycosylation is a common post-translational modification found throughout the GPCR family. The oligosaccharides in glycoproteins in general are believed to be important for facilitating protein folding and intracellular trafficking related to cell surface expression (*21, 22*). More recently, various studies have pointed to a role for glycosylation in direct regulation of GPCR function (*23*). The precise role of glycosylation in different classes of GPCRs is somewhat less clear, with variable effects on ligand binding, signal transduction, and cell surface expression (*24, 25*). Human RXFP1, like the glycoprotein hormone receptors, contains six predicted N-linked glycosylation sites in the ectodomain (*10*), including one site in the LDLa module. A number of studies have demonstrated that N-linked glycosylation of FSHR, LHR, and TSHR is important for intracellular trafficking of the receptors. Using HEK-293T cells stably expressing 7BP, which is a fusion protein consisting of the ectodomain of RXFP1 and the single-transmembrane (TM) domain of a T cell surface antigen CD8 (*10*), we have previously shown that the mass of the ectodomain protein, after cleavage from the single-TM domain, is consistent with post-translational modifications such as glycosylation (*26*). On the basis of the recent evidence pointing to glycosylation at site Asn-14 of the receptor being critical for ligand-directed downstream signaling and intracellular trafficking (*27*), we sought to investigate the degree of N-linked glycosylation of RXFP1 and to understand the role of glycosylation in RXFP1. To do this, we describe herein the effects of rational mutation (Asn to Gln or Ser to Ala) of the six potential N-linked glycosylation sites (Asn-X-Ser/Thr) in full-length RXFP1 on the extent of glycosylation, cAMP signaling, cell surface expression, and ligand binding.

MATERIALS AND METHODS

Sequence Alignments and Bioinformatic Analysis. Amino acid sequences of RXFP1 from human (Q9HBX9), orangutan (CAH92858), mouse (AAR97515), and rat (AAR97516) were retrieved from the GenBank database at NCBI. Sequence similarity searches of the available genomes at Ensembl using TBLASTN (*28*) using a representative full-length sequence of each receptor were conducted. Predicted orthologs of RXFP1 from the cow and opossum genomes, as well as the predicted RXFP1 ortholog from the dog, were identified. Sequences were aligned using ClustalW (*29*) with default parameters.

Homology Modeling of RXFP1's LRRs. The protein sequence corresponding to the majority of RXFP1's LRR-containing subdomain (residues 74−349) was submitted to Swiss-Model using the first approach mode (*30*). The PDB output was energy minimized with Deep View (*31*) for 1000 iterations at default settings. The quality of the homology model was assessed with ANOLEA (*32*) and WHATCHECK (*33*). Molsoft ICM-BrowserPro (Molsoft LLC) was used to analyze the model further and to generate image files.

Site-Directed Mutagenesis of RXFP1. The RXFP1 cDNA construct with an N-terminal FLAG tag in the pcDNA3.1/zeo mammalian expression vector has been described previously (*12*). Site-directed mutagenesis to create the mutants listed in Table 1 was performed on wild-type RXFP1 cDNA in the pcDNA3.1/zeo vector by PCR-based mutagenesis. Briefly, a pair of complementary primers, listed in Table 1, consisting of 25−40 bases were designed for each mutagenesis reaction with a change of asparagine to glutamine, or serine to alanine, placed in the middle of the primers. Wild-type RXFP1 inserted in pcDNA3.1 was used as the template DNA for PCR (GeneAmp Thermocycler, Applied Biosystems, Scoresby, Victoria, Australia) using Pfu DNA polymerase (Promega, Annandale, NSW, Australia) with the relevant primers, following the conditions, 95 °C for 30 s, 52 °C for 30 s, and 68 °C for 8 min, for 16 cycles. After digestion of the template plasmid DNA with 1 μL of *Dpn*I (Promega) at 37 °C for 1 h, the amplified plasmid DNA was transformed into *Escherichia coli* (DH-5α strain). Multiple-site RXFP1 mutants were constructed via introduction of additional mutations to the single-site RXFP1 mutants by site-directed mutagenesis. Individual clones were screened, and the identities of individual mutations were confirmed by DNA sequence on both strands; at the same time, the fact that there were no additional unwanted mutations in the full-length sequence of the receptor was confirmed.

Cell Culture and Transient Transfection in HEK-293T Cells. HEK-293T (human embryonic kidney) cells were grown in Dulbecco's modified Eagle's medium with 50 units/mL penicillin, 50 μg/mL streptomycin, and 2 mM glutamine supplemented with 10% fetal bovine serum at 37 °C in a humidified 5% CO_2/95% air incubator. Receptor cDNAs in pcDNA3.1/zeo were prepared using a Maxiplasmid DNA preparation kit (Invitrogen, Carlsbad, CA). Transfection was performed using Lipofectamine 2000 (Invitrogen) and OptiMEM serum-free medium (Gibco, Invitrogen) according to the manufacturer's protocols. Twenty-four hours later, immunoprecipitation−Western blotting analysis, a binding assay on intact cells, cell surface expression analysis, and cAMP assays were performed.

Immunoprecipitation and Immunoblot Analysis. Detergent-solubilized cell extracts from 4.5×10^6 transiently transfected cells were prepared using 1% Nonidet P-40 and 1% Triton X-100 in TBS [50 mM Tris (pH 7.4) and 150 mM NaCl] containing Complete Protease Inhibitor Cocktail Tablets (Roche Applied Science, Mannheim, Germany). Immunoprecipitation was performed using anti-FLAG M2 monoclonal antibody affinity gel (Sigma-Aldrich, Castle Hill, NSW, Australia) according to the manufacturer's instructions. One milliliter of cell lysate was gently agitated with 40 μL of prewashed suspending resin at 4 °C overnight. After incubation, the resin was washed with 1 mL of TBS three times. Proteins were eluted with NuPAGE 4× LDS sample buffer (Invitrogen). Recovered proteins were separated on NuPAGE Novex 4 to 12% Bis-Tris gels (Invitrogen) and analyzed by Western blot analysis using an anti-FLAG M2 monoclonal antibody−peroxidase conjugate (Sigma-Aldrich). Gel images were captured using an Epson Expression 1680 flat bed scanner and imported using Epson Twain Pro (Epson Pty, Sydney, Australia). Molecular weight analysis was performed using Syngene Gene Tools Software (Synoptics Ltd., Cambridge, U.K.).

Table 1: RXFP1 Mutants Utilized in This Study Showing the Consensus Sequence Mutated and the Primers Used To Generate the Mutation

Receptor mutant	Consensus sequence(s) disrupted	Primers used for each site (5'-3')
N14Q-RXFP1	Asn-14	*CCCCTGTGGGCAAATCACAAAGTGC;*
		GCACTTTGTGATTTGCCCACAGGGG
N105Q-RXFP1	Asn-105	*CGGTTTCTTCACAAGTGACTGCAATG;*
		CATTGCAGTCACTTGTGAAGAAACCG
N242Q-RXFP1	Asn-242	*CCATAATTTAAGACAATTGACTTTTATTTCC;*
		GGAAATAAAAGTCAATTGTCTTAAATTATGG
N250Q-RXFP1	Asn-250	*TTTCCTGCAGTCAATTAACTGTTTTAGTG;*
		CACTAAAACAGTTAATTGACTGCAGGAAA
N303Q-RXFP1	Asn-303	*GGAGCTGTCACAATTGCAACTTTCCTATAATCCAATCC;*
		GGATTGGATTATAGGAAAGTTGCAATTGTGACAGCTCC
S305A-RXFP1	Asn-303	*TGAATCTTGCCTATAATCCAATCCAGAAA;*
		GGATTATAGGCAAGATTCAATTGTGACAG
N346Q-RXFP1	Asn-346	*GACCTCTTATGCAACTCTCTCACATATATTTTAAG;*
		CTTAAAATATATGTGAGAGAGTTGCATAAGAGGTC
N105,242Q-RXFP1	Asn-105,242	
N105,250Q-RXFP1	Asn-105,250	
N242,250Q-RXFP1	Asn-242,250	
N105,242,250Q-RXFP1	Asn-105,242,250	
N105,250,S305A-RXFP1	Asn-105,250,303	
N105,250,346Q-RXFP1	Asn-105,250,346	

Glycosidase Treatment. Glycosidase treatment was performed on the receptor bound to anti-FLAG M2 monoclonal antibody affinity gel (Sigma-Aldrich). The beads with captured receptor were resuspended in 20 mM sodium phosphate buffer (pH 7.5) prior to *N*-glycosidase F (Roche) digestion, or 20 mM sodium phosphate buffer (pH 5.5) for endoglycosidase H (Roche) digestion. Proteins were denatured with 0.2% SDS, 1% NP-40, and 2% β-mercaptoethanol at 70 °C for 10 min. After denaturation, 1−2 units of *N*-glycosidase F or 2 milliunits of endoglycosidase H was added and the mixture incubated at 37 °C for 6 h. Samples were eluted from the affinity gel using NuPAGE 4× LDS sample buffer (Invitrogen), and Western blot analysis was performed as described above.

cAMP Measurements. Receptor cAMP signaling was assessed using a cAMP reporter gene assay (*19*). HEK-293T cells in 96-well plates were cotransfected with receptors and a pCRE-β-galactosidase reporter plasmid (*34*) in a ratio of 1:1 (courtesy of R. Cone, Disorders, Oregon Health and Science University, Portland, OR) to assess the cAMP signaling response to H2 relaxin. Transfected cells were incubated with increasing concentrations of H2 relaxin for 6 h, after which the medium was aspirated and the cells were frozen at −80 °C overnight. The amount of cAMP-driven β-galactosidase expression in each well was determined by incubating the cells in 25 μL of lysis buffer [10 mM Na_2HPO_4 (pH 8.0), 0.2 mM $MgSO_4$, and 0.01 mM $MnCl_2$] for 10 min and 100 μL of assay buffer [100 mM Na_2HPO_4 (pH 8.0), 2 mM $MgSO_4$, 0.1 mM $MnCl_2$, 0.5% Triton X-100, and 40 mM β-mercaptoethanol] for a further 10 min before 25 μL of enzyme/substrate solution [1 mg/mL chlorophenol red B-D galactopyranoside (Roche) in 100 mM Na_2HPO_4 (pH 8.0), 2 mM $MgSO_4$, and 0.1 mM $MnCl_2$] was added to each well and the plate incubated for 10 min. The absorbance of each well was determined at 570 nm using a Benchmark Plus microplate spectrometer (Bio-Rad, Hercules, CA). All experiments were repeated at least three times with triplicate determinations within each assay. Results are plotted as means ± the standard error of the mean of percent normalized response compared to 5 μM forskolin (Sigma-Aldrich). Data were analyzed with GraphPad Prism 4 (GraphPad Software, San Diego, CA), and a nonlinear regression sigmoidal dose−response (variable slope) model was used to plot curves and calculate pEC_{50} values. Final pooled pEC_{50} values and maximum response data were analyzed using one-way ANOVA coupled to Turkey's multiple-comparison test for multiple-group comparison.

Determination of the Levels of Receptor Total and Cell Surface Expression. The expression of wild-type (WT) and mutant RXFP1 receptors was assayed with an ELISA as previously described (*27*). Briefly, HEK-293T cells were plated into 24-well plates at a density of 2.8×10^5 cells/well and transfected with the receptor as described above. Twenty-four hours after transfection, cells were fixed with

3.7% (w/v) formaldehyde in TBS/$CaCl_2$ [50 mM Tris (pH 7.4), 150 mM NaCl, and 1 mM $CaCl_2$] for 15 min (for cell surface expression) or 3.7% (w/v) formaldehyde in TBS/$CaCl_2$ with the addition of 0.25% Triton X-100 (for total expression) and washed with TBS/$CaCl_2$ twice afterward. Cells were incubated with TBS/$CaCl_2$ containing 1% BSA for 45 min to block nonspecific binding and incubated with 10 μg/mL anti-FLAG M1 monoclonal antibody (Sigma-Aldrich) in TBS/$CaCl_2$ for 1 h at room temperature. Cells were then washed twice with TBS/$CaCl_2$ and reblocked with TBS/$CaCl_2$ containing 1% BSA for 15 min at room temperature before incubation with 2 μg/mL goat anti-mouse Alexa Fluor-488 (Invitrogen) in 200 μL of TBS/$CaCl_2$ containing 1% BSA for 1 h at room temperature. Cells were washed four times with TBS/$CaCl_2$ before the addition of 200 μL of lysis buffer [50 mM Tris (pH 7.4), 150 mM NaCl, 1 mM EDTA, and 1% Triton X-100]; 180 μL of the resultant solution from each well was transferred into a 96-well Optiplate (Perkin-Elmer, Boston, MA), and the fluorophore was excited at 490 nm and the emission recorded at 520 nm using time-resolved fluorometry in a Wallac Victor 3v multilabel counter (Perkin-Elmer). The value obtained from empty vector pcDNA3.1/zeo was used to determine nonspecific background. Data were normalized as means ± the standard error of the mean of the wild-type receptor percentage of triplicate measurements from at least three independent experiments. Final pooled expression data were analyzed using one-way ANOVA coupled to Tukey's multiple-comparison test for multiple-group comparison.

[^{33}P]H2 Relaxin Competitive Binding. Whole cell [^{33}P]H2 relaxin competitive binding assays were performed as previously described (*12*). Briefly, HEK-293T cells were plated into 24-well plates (2.8×10^5 cells/well) and transfected with the pcDNA3.1/zeo plasmid containing the receptor of interest the following day as described above. Twenty-four hours after transfection, competitive binding assays were performed with 100 pM [^{33}P]H2 relaxin in the absence or presence of increasing concentrations of unlabeled relaxin (up to 500 nM). Data are presented as means ± the standard error of the mean of the percentage of specific binding from at least three independent experiments performed in triplicate. Data were analyzed using GraphPad Prism 4, and a nonlinear regression one-site binding model was used to plot curves and calculate pIC_{50} values. The final pooled pIC_{50} was analyzed using one-way ANOVA coupled to Turkey's multiple-comparison test for multiple-group comparison.

RESULTS

Potential N-Linked Glycosylation Sites Are Conserved in RXFP1 from Different Species. Analysis of the primary sequence of RXFP1 using NetNGlyc 1.0 reveals the presence of six potential glycosylation sites at positions Asn-14, -105, -242, -250, -303, and -346 of the mature RXFP1 protein sequence (Table 2). Asn-14 is located in the LDLa module at the N-terminus, whereas the rest are localized in the putative LRR region. We have used a modeling approach to localize the position of the glycosylation sites within the LRR structure. BlastP alignment of the predicted LRRs of RXFP1 (residues 74−349) revealed that its closest homologue is the Nogo receptor (NgR), exhibiting a sequence 47% similar and 31% identical to that of the LRRs of RXFP1 (*17*). This sequence homology is predominantly ascribed to conserved residues contained in the 24-amino acid "typical-type" LRR consensus sequence (LxxLx<u>xLx</u>LxxNxLxxLxxxoFxx, where x represents any residue, o represents any nonpolar residue, and the β-strand is underlined) (*35, 36*). Residues 74−349 of RXFP1 were submitted to Swiss-Model using the first approach mode (*30*). The resultant structure was modeled on three known structures, two crystal structures of the NgR [Protein Data Bank (PDB) entries 1OZN and 1P8T] and the crystal structure of biglycan (PDB entry 2FT3). The model of RXFP1's LRRs (Figure 1A) exhibited a Ramachandran *Z* score of −0.525, indicating that the structure is reasonable. The model suggests that the LRRs of RXFP1 fold into a banana-like conformation similar to the structure of NgR. This structure allowed us to predict the locations of the potential N-linked glycosylation sites throughout the LRR superstructure of RXFP1. Asn-105 is located at position 3 of LRR I, in the center of the loop preceding the β-strand. Being in position 19 of LRR VI, Asn-242 is located on the outer, convex ridge of the LRR superhelix. Asn-250 is in position 3 of LRR VII, in the center of the loop preceding the β-strand of LRR VII. Asn-303 occupies the final position of the β-strand in LRR IX, exposed in the middle of the large concave β-sheet of the LRR solenoid. Asn-346 is located in the C-terminal cap of the LRRs. Analysis of the homology model of RXFP1's LRRs in ICM-BrowserPro indicates that all the asparagine residues are exposed on the surface of the structure. We examined whether any of these six sites are conserved in RXFP1 sequences from other mammalian species. We were able to identify RXFP1 sequences from human, chimpanzee, mouse, rat, cow, dog, and opossum genomes. As shown in Figure 1B, sites 1−3, 5, and 6 (Asn-14, -105, -242, -303, and -346, respectively) are highly conserved in all seven mammalian species, and site 4 (Asn-250) is present in six species.

Table 2: Prediction of the N-Linked Glycosylation Sites in RXFP1 Using NetNGlyc 1.0[a]

position	potential	N-Glyc result
14 NITK	0.8119	+++
105 NVTA	0.6217	+
242 NLTF	0.5483	+
250 NLTV	0.7111	++
303 NLSY	0.6656	++
346 NLSH	0.6374	+

[a] Six potential N-linked glycosylation sites at positions Asn-14, -105, -242, -250, -303, and -346 were revealed and their probabilities of glycosylation ranked.

Enzymatic Digestion of RXFP1. A glycosylation analysis program NetNGlyc (www.cbs.dtu.dk/services/NetNGlyc) predicts that RXFP1 has six N-linked sites, but no O-linked glycosylation sites. To show that RXFP1 is indeed glycosylated, the receptor which contains a FLAG epitope fused to the N-terminus transiently expressed in HEK-293T cells was immunoprecipitated using anti-FLAG M2 monoclonal antibody affinity gel and enzymatic deglycosylation performed in situ. Following elution with SDS−PAGE sample buffer, proteins were separated on NuPAGE Novex 4 to 12% Bis-Tris gels and RXFP1 specifically detected by Western blot analysis using the anti-FLAG M2 monoclonal antibody (Figure 2). Wild-type RXFP1 protein was detected as a broad, slightly diffuse band migrating from 80 to 85 kD as

A.

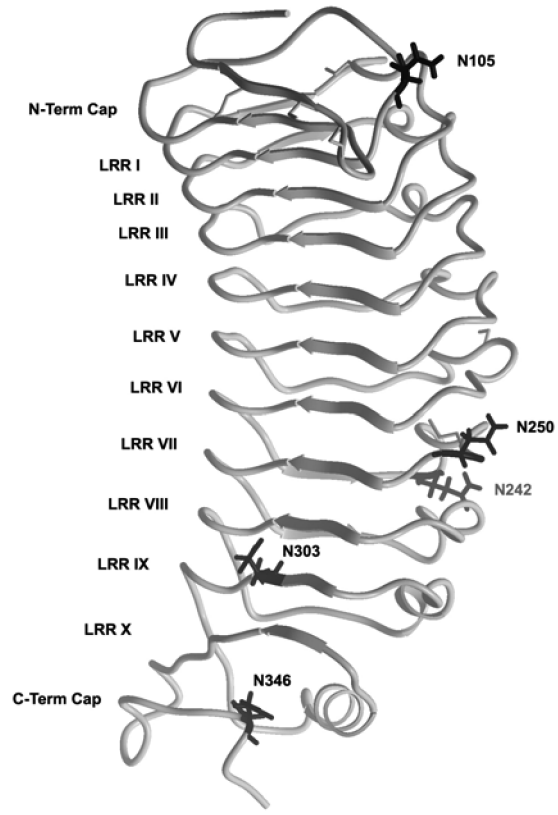

B.

	site 1: Asn-14	site 2: Asn-105	site 3: Asn-242
Human RXFP1	FPCGNITKCLP	PSVSSNVTAMS	NHIHNLRNLTF
Chimp RXFP1	FPCGNITKCLP	PSVSSNVTAMS	NHIHNLRNLTF
Mouse RXFP1	FPCGNMSRCLP	PSVSSNVTVMS	NRIHNLRNLTF
Rat RXFP1	FPCGNISKCLP	PSVSSNVTVMS	NRIHNLRNLTF
Dog RXFP1	FPCGNLTKCLP	PSVSSNVTLMS	NHIHNLRNLTF
Bovine RXFP1	FPCGNTTKCLP	PSVSSNVTFMS	-HIHNLRNLTF
Oposs RXFP1	FPCGNATKCLP	PSVSSNVTMMS	NHIHNLRNMTF
	10 20	100 110	235 245

	site 4: Asn-250	site 5: Asn-303	site 6: Asn-346
Human RXFP1	ISCSNLTVLVM	LSQLNLSYNPI	FRPLMNLSHIY
Chimp RXFP1	ISCSNLTVLVM	LSQLNLSYNPI	FRPLMNLSHMY
Mouse RXFP1	ISCNNLTVLVM	LSQLNISYNPI	FRPLINLSHIY
Rat RXFP1	ISCNNLTVLEM	LSQLNISYNPI	FRPLINLSHIY
Dog RXFP1	ISCGNLTVLVM	LSQLNLSYNPI	FRPLMNLSHIY
Bovine RXFP1	ISCSNLTVLVM	LQKLNLSYNPI	FRPLMNLSYMY
Oposs RXFP1	ISCSTLTVLVM	LSQLNLSYNPI	FAPLRNLSHMY
	246 256	299 309	341 351

FIGURE 1: Localization and conservation of glycosylation sites in the RXFP1 ectodomain. (A) Structural representation of the localization of N-linked glycosylation sites based on a model of the RXFP1 leucine-rich repeats (LRRs) derived from the Nogo receptor ectodomain crystal structure (*36*). Asn-105, Asn-242, Asn-250, and Asn-303 are located within the LRRs, whereas Asn-346 is located in the C-terminal cap of the LRRs. (B) Alignment of RXFP1 sequences from seven different mammalian species showing N-linked glycosylation sites 1−6 and surrounding sequences. Amino acid residue numbers are based on the mature human RXFP1 protein sequence.

previously reported (*37*). Regression analysis of the band using Syngene Gene Tools Software indicated an apparent molecular mass of approximately 82 kDa. Treatment of wild-type RXFP1 with *N*-glycosidase F or endoglycosidase H both decreased the size and heterogeneity of the band, resulting in an apparent size of approximately 61 kDa. This change in molecular mass suggests that multiple sites are glycosylated. More importantly, wild-type RXFP1 detected by immunoblot was sensitive to both Endo H and PNGase F treatment, indicating that the immunoprecipitated RXFP1

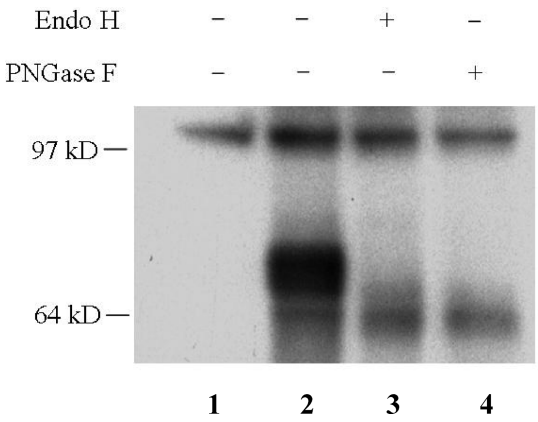

FIGURE 2: Western blot analysis of RXFP1 transiently expressed in HEK-293T cells and effects of glycosidase treatment. RXFP1 immunoprecipitated from HEK-293T cell extracts using anti-FLAG M2 affinity agarose migrates as a broadband with an apparent molecular mass of 82 kDa. Proteins were probed with an anti-FLAG M2 monoclonal antibody−peroxidase conjugate. Treatment with endoglycosidases, PNGase F or Endo H, induces a clear decrease in the apparent molecular mass of RXFP1: lane 1, transfected with empty pcDNA3.1/zeo vector; lanes 2−4, WT-RXFP1.

band was the precursor form of the receptor containing high-mannose-type oligosaccharides (Figure 2).

Identification of Actual N-Linked Glycosylation Sites of RXFP1. To determine which of the potential N-linked sites were glycosylated, we generated a series of mutant RXFP1 cDNA expression vectors in which one or more of the six potential glycosylation sites were mutated. The wild-type and mutant proteins were expressed in HEK-293T cells by transient transfection, and their electrophoretic mobilities were determined by immunoprecipitation, SDS−PAGE, and immunoblot analysis using the anti-FLAG antibody. The expectation was that there would be a small increase in electrophoretic mobility in the mutant RXFP1 receptors relative to the wild type if the mutated site were glycosylated. Direct comparison of the mobility of immunoblot bands revealed subtle but reproducible differences for all of the single-site glycosylation-defective mutants: N14Q, N105Q, N242Q, N250Q, N303Q, and N346Q (Figure 3A, lanes 3−8, respectively). Analysis of the individual bands using Syngene Gene Tools Software indicated a reduction in molecular size of 2−3 kDa compared to the wild-type receptor, compatible with a loss of high-mannose-type oligosaccharides at a single site. Therefore, it was likely that each potential N-glycosylation site was actually utilized.

This observation is further supported by immunoblot analysis of mutants in which multiple potential sites were serially disrupted. As one can see in Figure 3B, mutants containing an increasing number of glycosylation-defective sites showed a ladderlike increase in mobility. Syngene Gene Tools Software analysis of the adjacent bands again revealed a reduction in molecular size of ~3 kDa for each of the bands, suggesting that each site was indeed N-glycosylated. The triple site mutant N104,242,250Q-RXFP1 was not detected by immunoprecipitation−Western blotting analysis.

Functional Analysis of the Effect of Disruption of Individual N-Linked Glycosylation Sites. To investigate the functional ramifications of the loss of each glycosylation site, plasmids containing each individual mutation of the receptor were transfected into HEK-293T cells, and the functional characteristics of the mutant and wild-type receptors were examined by measurement of cAMP activity after stimulation with different concentrations of H2 relaxin. No significant difference was observed in the potency (pEC_{50}) and maximum response (% forskolin response) between the mutants with individual disruption at sites Asn-242, Asn-250, and Asn-346 and the wild-type receptor (Figure 4 and Table 3). In contrast, mutation at site Asn-105 significantly decreased the maximum response without affecting the pEC_{50} (Figure 4 and Table 3). More drastic impairment of signaling function was observed on N14Q-RXFP1 and N303Q-RXFP1 with significant reduction in both pEC_{50} and maximum response, especially for the mutation at site Asn-303 which showed an 100-fold reduced potency of cAMP production compared to that of the wild-type receptor (Figure 4 and Table 3). To confirm that the reduced pEC_{50} of N303Q-RXFP1 is due to the loss of the N-linked glycosylation at site Asn-303, rather than the change of the amino acid residue from Asn to Gln, we constructed another related mutant, S305A-RXFP1, which ablates the glycosylation at the same site as N303Q-RXFP1 by disruption of the N-linked glycosylation consensus sequence NXS/T. This mutant was also found to have reduced cAMP activity with a pEC_{50} similar to that observed for N303Q-RXFP1 (Figure 4 and Table 3). However, it is worth noting that S305A-RXFP1 exhibited an unchanged maximum response compared to the wild-type receptor.

The diminished activities of the single-glycosylation site-defective mutants could be due to a reduction in receptor presentation to the cell surface, binding affinity, or G-protein coupling. To distinguish among these possibilities, we next carried out an ELISA, using recognition of the FLAG-epitope sequences at the N-termini of the constructs, to determine the the level of cell surface expression compared to the total level of expression. It can be seen (Figure 5) that mutation at sites Asn-242, Asn-250, Ser-305, and Asn-346 of RXFP1 resulted in cell surface expression similar to that of the wild-type receptor. These mutants all also exhibited a similar maximum cAMP response to the wild-type receptor (Figure 4 and Table 3), indicating that these individual mutants were expressed on the cell surface at levels comparable with that of wild-type RXFP1. In contrast, mutation at sites Asn-14, Asn-105, and Asn-303 resulted in 62.10 ± 4.4% ($P < 0.001$), 66.91 ± 5.3% ($P < 0.001$), and 50.49 ± 6.2% ($P < 0.001$) of the cell surface expression, respectively, compared with that of the wild-type receptor (Figure 5), which reflects the decreased maximum cAMP production observed in the cAMP assay (Figure 4). Importantly, S305A-RXFP1 demonstrated cell surface expression equivalent to that of the wild-type receptor which reflected its unchanged maximum cAMP response.

To determine the total level of receptor expression (i.e., cell surface and intracellular), we measured receptor levels, using the ELISA, after permeabilization of cells with Triton X-100. Mutants N14Q-RXFP1 and N303Q-RXFP1 exhibited compromised total expression levels with reduction to 83.68 ± 1.9% ($P < 0.05$) and 52.51 ± 1.6% ($P < 0.001$) of the wild-type receptor levels, respectively, while the rest of the single-site mutants showed total expression levels of the receptors comparable to that of the wild type (Figure 5). Importantly, S305A-RXFP1 demonstrated total and cell surface expression equivalent to that of the wild-type receptor, suggesting that the reduced total and cell surface expression levels observed for N303-RXFP1 were due to

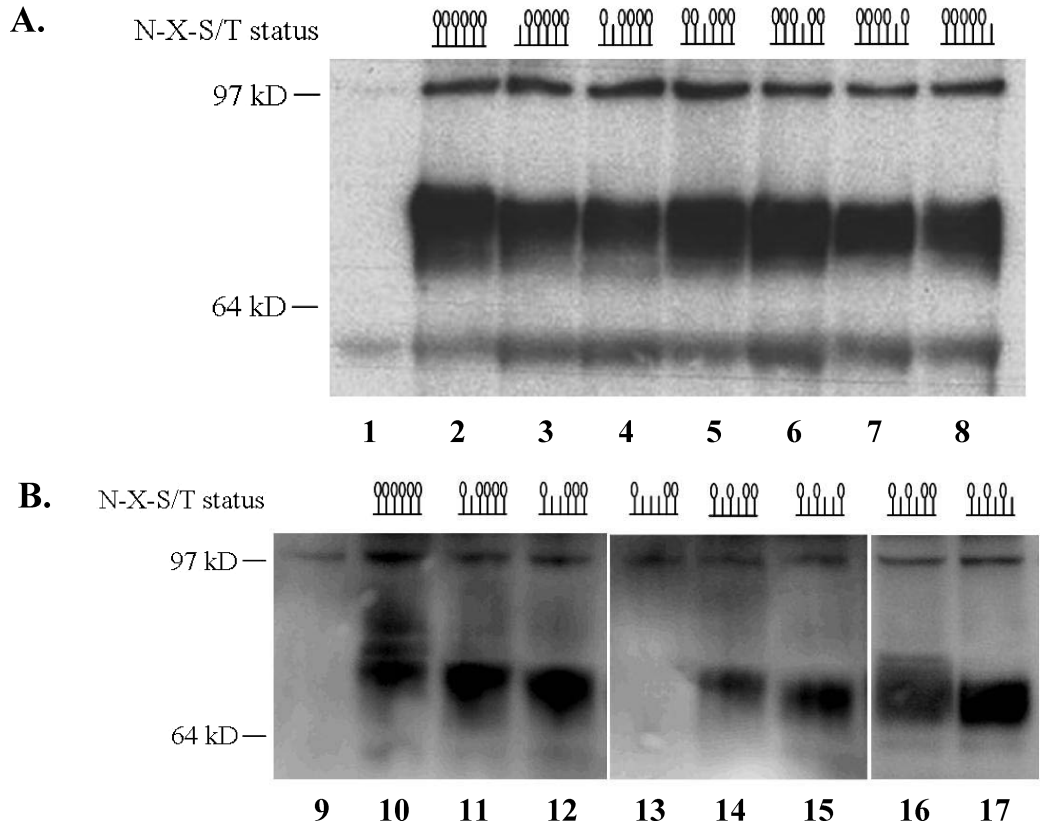

FIGURE 3: Western blotting of RXFP1 mutants to identify the N-linked glycosylation sites. Wild-type RXFP1 and glycosylation-defective mutants of RXFP1 were transiently expressed in HEK-293T cells. Detergent-solubilized extracts of HEK-293T cells were immunoprecipitated with anti-FLAG M2 affinity agarose. Proteins were probed with an anti-FLAG M2 monoclonal antibody−peroxidase conjugate. (A) WT-RXFP1 and RXFP1 mutants at a single putative N-linked glycosylation site: lane 1, empty pcDNA3.1/zeo vector; lane 2, WT-RXFP1; lane 3, N14Q-RXFP1; lane 4, N105Q-RXFP1; lane 5, N242Q-RXFP1; lane 6, N250Q-RXFP1; lane 7, N303Q-RXFP1; and lane 8, N346Q-RXFP1. (B) WT-RXFP1 and RXFP1 mutants at multiple putative N-linked glycosylation sites: lane 9, empty pcDNA3.1/zeo vector; lane 10, WT-RXFP1; lane 11, N105Q-RXFP1; lane 12, N105,242Q-RXFP1; lane 13, N105,242,250Q-RXFP1; lane 14, N105,250Q-RXFP1; lane 15, N105,250Q,S305A-RXFP1; lane 16, N105,250Q-RXFP1; and lane 17, N105,250,346Q-RXFP1.

the individual amino acid residue change rather than the loss of glycosylation per se. In contrast, mutants N14Q-RXFP1 and N105Q-RXFP1 demonstrated compromised delivery of their receptors, indicating that N-linked glycosylation at Asn-14 and Asn-105 is important for regulation of the receptor trafficking to the plasma membrane.

We next investigated whether the decreased pEC_{50} values that we had observed for some mutants (Figure 4 and Table 3) were in part due to reduced ligand binding affinity. The mutant receptor constructs were transiently expressed in HEK-293T cells and were individually characterized by [^{33}P]H2 relaxin competitive binding. All the individual N-linked glycosylation site mutants demonstrated binding affinity for H2 relaxin similar to that of the wild-type receptor (Figure 6 and Table 3), suggesting glycosylation at each site was not necessary for binding of H2 relaxin to the receptor.

Functional Analysis of the Effect of Disruption of Multiple N-Linked Glycosylation Sites. On the basis of our analysis of the location of the six glycosylation sites, we further investigated the functional effect of elimination of glycosylation at multiple sites. As described above, Asn-105, Asn-242, Asn-250, Asn-303, and Asn-346 were all located in the LRR domain, so we designed a series of mutants combining adjacent glycosylation sites based on the structural model of the LRRs (Figure 1) to probe the functional ramifications of changes at multiple sites in concert. Therefore, we constructed double site mutants N105,242Q-RXFP1, N105,250Q-RXFP1, N242,250Q-RXFP1, and N303,346Q-RXFP1. The expectation was that the multiple-site mutations would influence either the potency of H2 relaxin-stimulated cAMP activity (pEC_{50}), receptor delivery to the plasma membrane, or ligand binding affinity by comparison with the corresponding single-site mutants if the glycosylation at those multiple sites functions in concert. Two double site mutants, N105,242Q-RXFP1 (Figure 7A) and N242,250Q-RXFP1 (Figure 7C), exhibited reduced pEC_{50} values compared to those of the corresponding single-site mutants (Table 3). The other two double site mutants, N105,250Q-RXFP1 (Figure 7E) and N303,346Q-RXFP1 (Figure 7G), exhibited pEC_{50} values similar to those of the corresponding single-site mutants. N242,250Q-RXFP1 was the only mutant which demonstrated a significantly reduced maximum cAMP response compared to the corresponding single-site mutant, which was consistent with the significantly reduced cell surface expression level detected for this receptor (Figure 7D). Clearly, the combination of Asn-242 and Asn-250 is necessary for optimal cell surface expression, although the combinations of Asn-105 and Asn-242 as well as Asn-105 and Asn-250 also exhibited a lower level of cell surface expression, but this was not statistically significant.

Importantly, removal of all the these three glycosylation sites, Asn-105, Asn-242, and Asn-250, resulted in a non-functional receptor, N105,242,250Q-RXFP1 (Figure 8A and Table 3). This mutant exhibited a dramatically reduced total

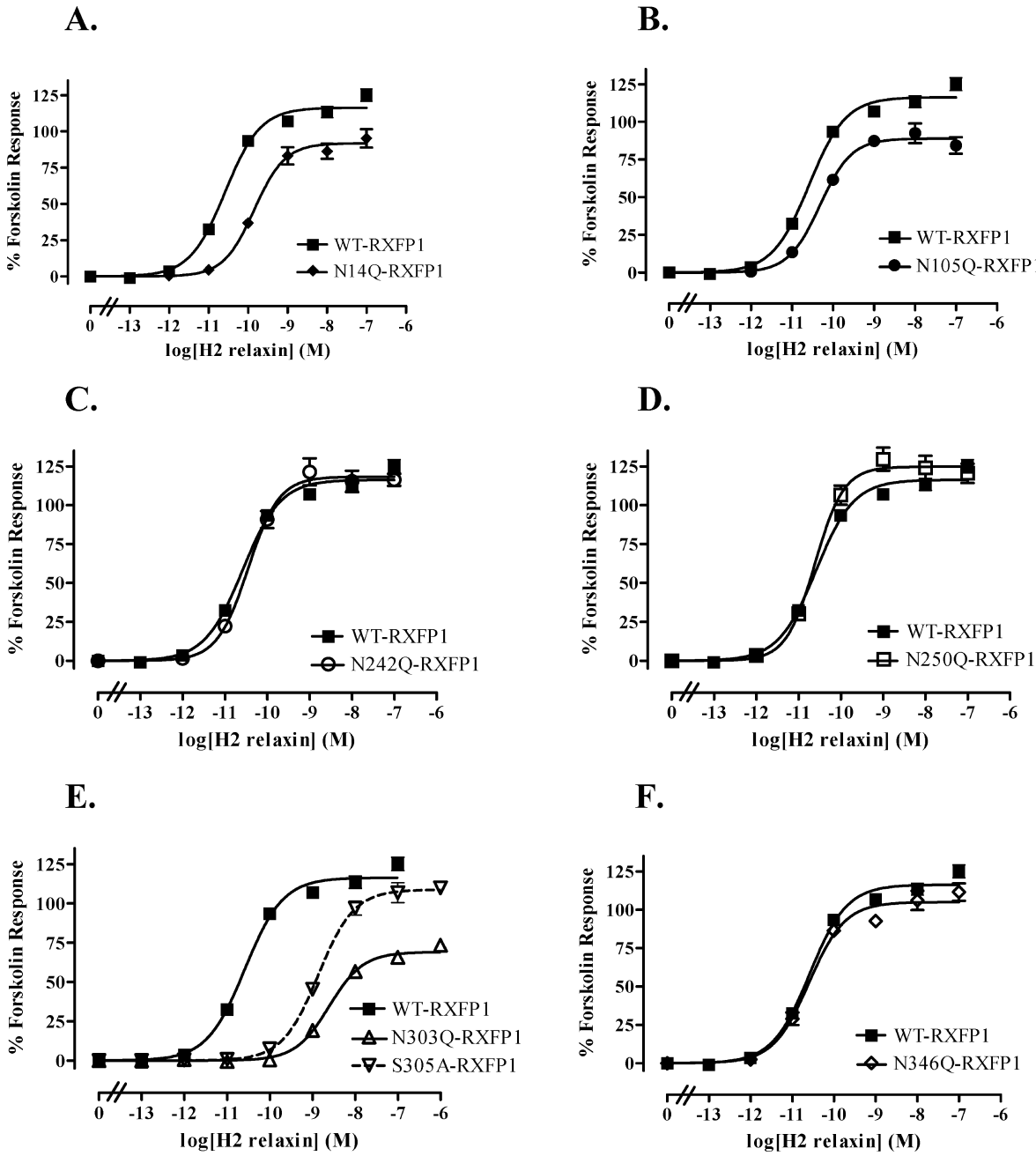

FIGURE 4: H2 relaxin-stimulated cAMP activity response in WT-RXFP1 compared to RXFP1 mutants at a single glycosylation site. cAMP activity is expressed as a percentage of the 5 μM forskolin-stimulated response for each receptor. Symbols represent means, and vertical bars represent standard errors of triplicate determinations from at least three experiments.

expression level compared with the wild-type receptor (Figure 8B), which was in a good agreement with the immunoprecipitation−Western blotting analysis during which no receptor bands were detected (Figure 3B). Importantly, the cell surface expression of the mutant was not different from background, indicating that the receptor was not expressed at the cell surface. Consistent with this observation, N105,242,250Q-RXFP1 was not able to bind [^{33}P]H2 relaxin at a concentration of 100 pM in whole cell comparative binding assays (Figure 9A). Hence, the combination of these sites was essential for cell surface expression.

To further study the combined effects of the mutation of multiple glycosylation sites, two other triple-site mutants, N105,250Q,S305A-RXFP1 and N105,250,346Q-RXFP1, were constructed and analyzed. N105,250Q,S305A-RXFP1 exhibited a further significantly reduced pEC_{50} value compared to S305A-RXFP1 (Figure 8C and Table 3). Similarly, N105,250,346Q-RXFP1 resulted in a significantly reduced pEC_{50} value compared to that of either N105,250Q-RXFP1 or N346Q-RXFP1 alone (Figure 8E and Table 3). The maximum cAMP response of both the triple mutants was similar to that of double-site mutant N105,250Q-RXFP1, which correlated with the comparable cell surface expression levels of the two triple-site mutants to N105,250Q-RXFP1 (Figure 8D,F and Table 3). To determine whether the decreased pEC_{50} values that we had observed for mutants N105Q-RXFP1, 242Q-RXFP1, N105, 250Q-RXPF1, S305A-RXFP1, and N105, 250, 346Q-RXFP1 were partly due to a reduction in the ligand binding affinity, whole cell competition binding assays were conducted. All these mutants demonstrated similar binding affinity for H2 relaxin compared to that of the wild-type receptor (Figure 9B−E and

Table 3: cAMP Activity Data, Including pEC_{50} and Maximum Values Expressed as a Percentage of 5 μM Forskolin Stimulation [Max (% F)], and Competition Binding Data Showing pIC_{50} Values for the Wild-Type and Glycosylation-Defective RXFP1 Receptors[a]

receptor	pEC_{50}	Max (% F)	*n*	pIC_{50}	*n*
WT-RXFP1	10.57 ± 0.06	124.30 ± 4.24	16	9.42 ± 0.11	10
N14Q-RXFP1	9.86 ± 0.11[c]	95.26 ± 6.35[b]	5	8.90 ± 0.28	3
N105Q-RXFP1	10.36 ± 0.17	84.35 ± 5.42[c]	3	9.43 ± 0.38	3
N242Q-RXFP1	10.44 ± 0.08	116.40 ± 3.86	5	9.34 ± 0.43	3
N250Q-RXFP1	10.62 ± 0.04	120.50 ± 6.25	4	9.14 ± 0.09	3
N303Q-RXFP1	8.67 ± 0.14[c]	82.50 ± 6.26[c]	4	8.99 ± 0.44	3
S305A-RXFP1	8.85 ± 0.11[c]	106.80 ± 6.32	4	9.09 ± 0.09	3
N346Q-RXFP1	10.55 ± 0.18	111.60 ± 5.64	3	9.60 ± 0.16	3
N105,242Q-RXFP1	9.66 ± 0.08[d]	89.14 ± 89.14	3	9.64 ± 0.15	3
N105,250Q-RXFP1	10.15 ± 0.09	85.84 ± 2.73	5	ND	
N242,250Q-RXFP1	10.08 ± 0.06[e]	97.57 ± 3.73[e]	3	9.17 ± 0.05	3
N303,346Q-RXFP1	8.20 ± 0.09	74.61 ± 4.36	3	ND	
N105,242,250Q-RXFP1	NR	0.53 ± 0.48[h]	4	NA	3
N105,250Q,S305A-RXFP1	7.57 ± 0.21[f]	67.09 ± 6.58	3	9.35 ± 0.07	3
N105,250,346Q-RXFP1	9.26 ± 0.25[g]	82.17 ± 2.84	3	9.59 ± 0.21	3

[a] Data are means ± the standard error of the mean from more than three independent experiments each performed in triplicate. NR means no response, NA no affinity, and ND not determined. [b] $P < 0.01$. [c] $P < 0.001$ vs WT-RXFP1. [d] $P < 0.01$ vs N105Q-RXFP1. [e] $P < 0.05$ vs N242Q-RXFP1. [f] $P < 0.001$ vs S305A-RXFP1. [g] $P < 0.01$. [h] $P < 0.001$ vs N105,250Q-RXFP1 (one-way ANOVA and Tukey's multiple-comparison test).

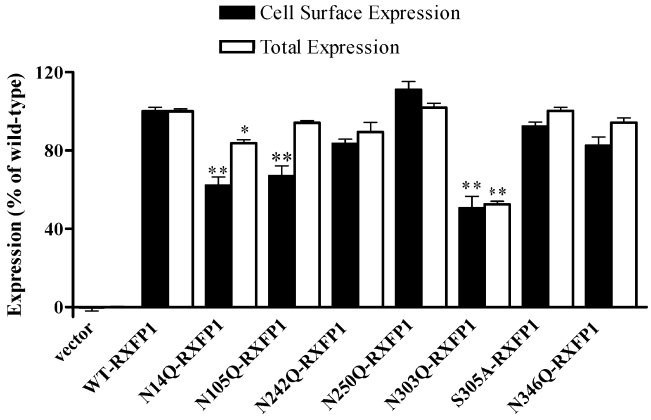

FIGURE 5: Comparison of expression of WT-RXFP1 and RXFP1 mutants at a single glycosylation site transiently expressed in HEK-293T cells. The level of receptor expression is determined by an ELISA using the an anti-FLAG M1 monoclonal antibody to the FLAG epitope on whole cells. The amount of cell surface (black column) and total (white column) expression are presented as a percentage of the amount of wild-type RXFP1 expression with empty vector transfected HEK-293T cells being used to define 0%. Data are means ± the standard error of the mean from more than five experiments performed in triplicate. (*) $P < 0.05$, and (**) $P < 0.001$ vs WT-RXFP1 (one-way ANOVA and Tukey's multiple-comparison test).

Table 3). Importantly, these results demonstrated that glycosylation at multiple sites was not necessary for primary H2 relaxin binding but that combinations of Asn-105, Asn-250, Asn-303, and Asn-346 were essential for cAMP signaling.

DISCUSSION

Analysis of the primary sequence of the human RXFP1 receptor predicted six putative N-linked glycosylation sites in the ectodomain (*10*). In our previous studies on the isolated RXFP1 ectodomain (7BP) expressed in HEK-293T cells, we showed that the mass of the soluble ectodomain protein observed by SELDI analysis was consistent with post-translational modifications, suggesting glycosylation of the receptor ectodomain (*26*). We have also demonstrated that the predicted glycosylation site on the RXFP1 LDLa module (Asn-14) is glycosylated in vitro (*19*). Recently, it has been shown that glycosylation at Asn-14 is important for signal transduction and cell surface delivery of the receptor (*27*). In this study, we have investigated the role of all of the potential glyosylation sites in the RXFP1 ectodomain, especially the sites in LRRs both alone and in combination.

First, to prove the full-length receptor is N-glycosylated, we used the well-characterized deglycosylation enzymes PNGase F and Endo H to treat immunoprecipitated RXFP1 protein. Endo H cleaves asparagine-linked high-mannose and hybrid, but not complex, oligosaccharides from glycoproteins, whereas PNGase F cleaves all types of asparagine-linked oligosaccharides from glycoproteins. Prior to enzyme digestion, the broad immunoblot band of RXFP1 showed an average apparent mass of 82 kDa, which is consistent with the size of FLAG-tagged RXFP1 which we have reported previously (*37*). Enzymatic digestion of RXFP1 resulted in a decrease in the apparent size of the immunoprecipitated protein band, clearly indicating that the receptor is glycosylated. The reduction in the molecular mass from 82 to 61 kDa is in good agreement with the molecular mass of N-linked oligosaccharides calculated in our previous study on the isolated RXFP1 ectodomain (*26*).

Enzymatic digestion of RXFP1 with both PNGase F and Endo H treatment resulted in a band of identical size, indicating that the oligosaccharides in the immunoprecipitated RXFP1 protein were high-mannose or hybrid-type. This is indicative of the immunoprecipitated RXFP1 protein not having been processed through the Golgi and hence being the immature form of the receptor. In support of this, a recent study demonstrated that HA-tagged wild-type RXFP1 expressed in HEK-293T cells was detected via Western blotting as two molecular mass forms using anti-HA antibody (*27*). The lower-molecular mass band had a similar molecular mass to the major immunoblot band of 82 kDa seen in our studies. The higher-molecular mass band was Endo H resistant, suggesting that it contained complex-type N-linked glycosylation compatible with it being the mature form of the receptor. The lower-molecular mass band was reduced to a size similar to that we had observed in our studies following treatment with both PNGase F and Endo H (61 kDa). This strongly suggests that the immunoprecipitated RXFP1 band utilizing anti-FLAG M2 affinity agarose used in our studies was a precursor form of the receptor containing high-

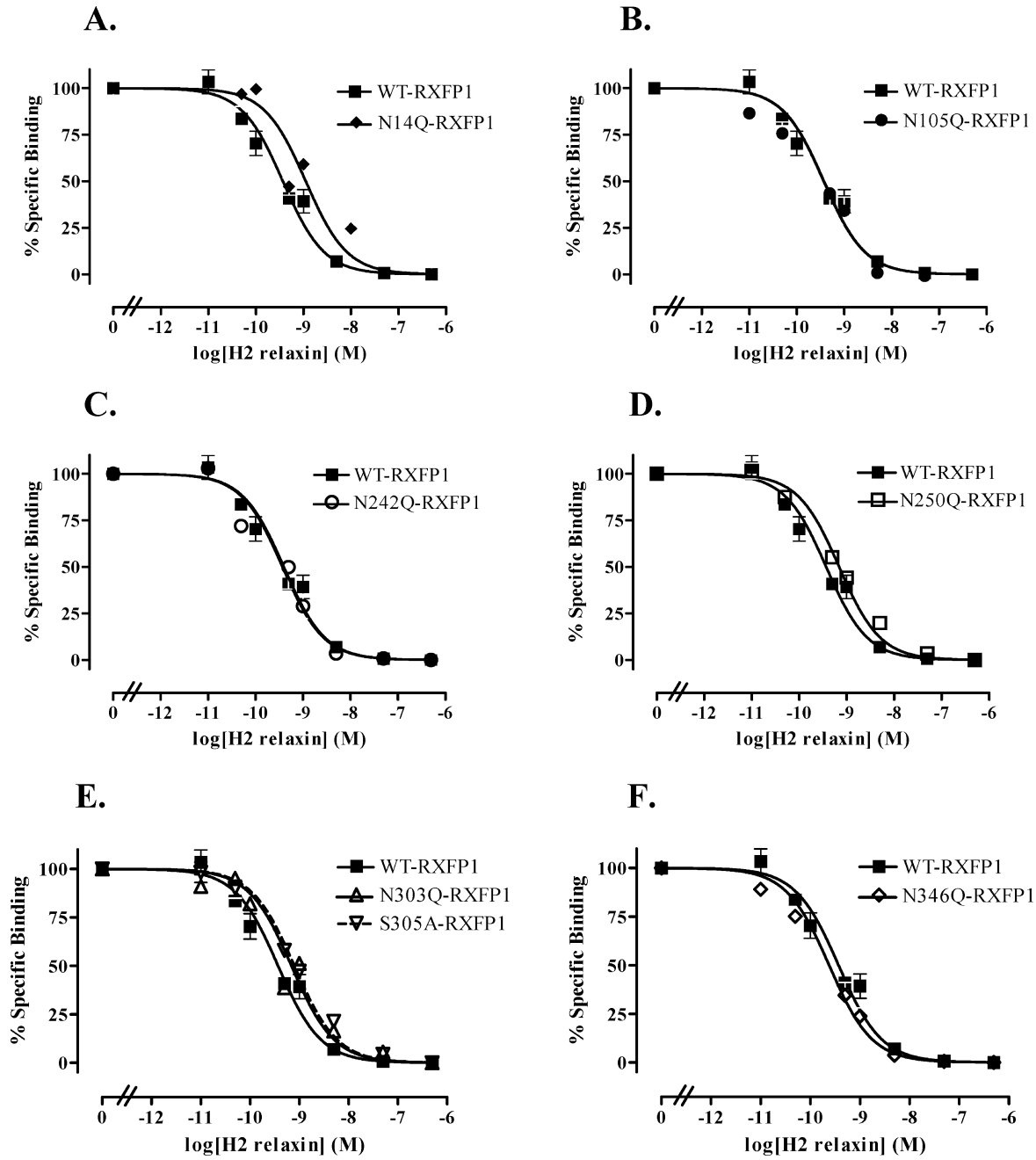

FIGURE 6: Competition binding curves using [^{33}P]H2 relaxin comparing the H2 relaxin binding affinities of single-glycosylation site mutants to that of WT-RXFP1: (A) N14Q-RXFP1, (B) N105Q-RXFP1, (C) N242Q-RXFP1, (D) N250Q-RXFP1, (E) N303Q-RXFP1, and (F) N346Q-RXFP1. Symbols represent means, and vertical bars represent standard errors of the mean of three individual experiments performed in triplicate.

mannose-type N-linked glycosylation, whereas the mature form of the receptor was not detected. Clearly, the FLAG-tagged receptors in this study are being expressed at the cell surface as demonstrated by the cAMP activity, cell surface expression, and ligand binding assays. The reason for the lack of mature cell surface receptors in our immunoprecipitations is unknown. Interestingly, a previous study of glycosylation of FLAG-tagged LHR expressed in HEK-293T cells also showed very small amounts of the mature form of the receptor compared to the immature form after immunoprecipitation with the anti-FLAG antibody (*38*). Importantly, our studies were designed to demonstrate that the potential glycosylation sites are indeed utilized in the full-length receptor which is adequately highlighted by studying the immature form of the receptor with high-mannose glycosylation.

We demonstrated that all six putative N-linked glycosylation sites on the RXFP1 ectodomain were actually glycosylated in HEK-293T cells by using a series of RXFP1 mutants with different glycosylation status. The minor size shifts of the immunoprecipitated bands and the homogeneity of the band size seen in the single-site mutants are consistent with the precursor form of the receptor containing high-mannose-type glysosylation, as each simple and nonbranched N-linked glycochain contributes up to ~3.5 kDa to a protein (*39*). Our observation of six actually glycosylated sites in RXFP1 fully accounts for the discrepancy in its molecular masses after enzymatic deglycosylation treatment (from 82 to 61 kDa).

The functional effects of N-glycosylation on GPCRs are highly variable. For some receptors, such as the AT2

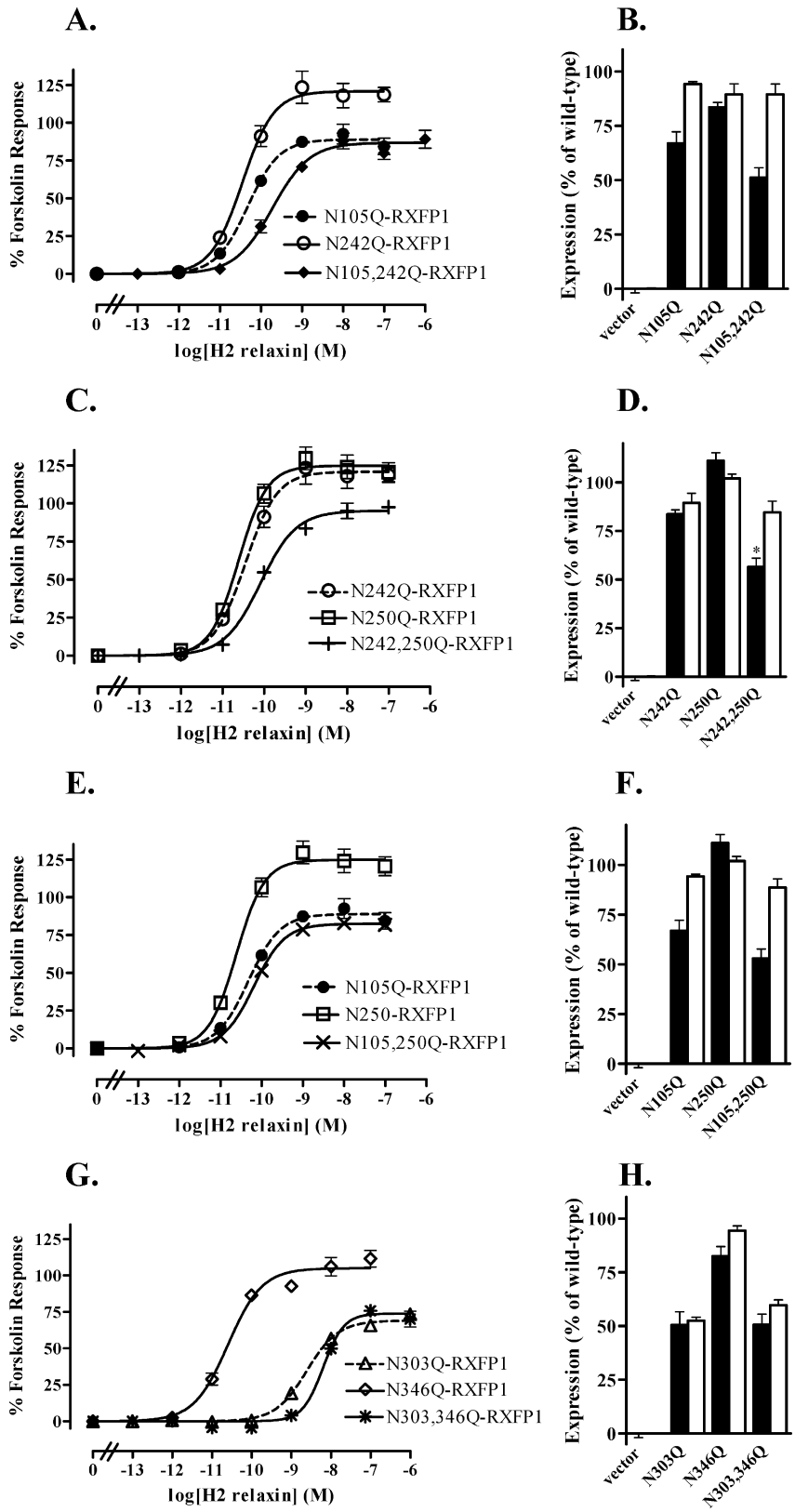

FIGURE 7: H2 relaxin-stimulated cAMP activity responses (A, C, E and G) and receptor expression (B, D, F, and H) of RXFP1 mutants at two glycosylation sites compared to the respective single-site mutants: (A and B) N105,242Q-RXFP1 compared to N105Q-RXFP1 and N242Q-RXFP1, (C and D) N242,250Q-RXFP1 compared to N242Q-RXFP1 and N250Q-RXFP1, (E and F) N105,250Q-RXFP1 compared to N105Q-RXFP1 and N250Q-RXFP1, and (G and H) N303,246Q-RXFP1 compared to N303Q-RXFP1 and N346Q-RXFP1. cAMP activity is expressed as a percentage of the 5 μM forskolin-stimulated response for each receptor. The level of cell surface expression is determined by an ELISA using the anti-FLAG M1 monoclonal antibody to the FLAG epitope on whole cells. The amount of cell surface (black column) and total (white column) expression are presented as a percentage of the amount of wild-type RXFP1 expression with empty vector transfected HEK-293T cells being used to define 0%. Symbols represent means, and vertical bars represent standard errors of the mean of more than three experiments. (*) $P < 0.01$ compared to N242Q-RXFP1 (one-way ANOVA and Tukey's multiple-comparison test).

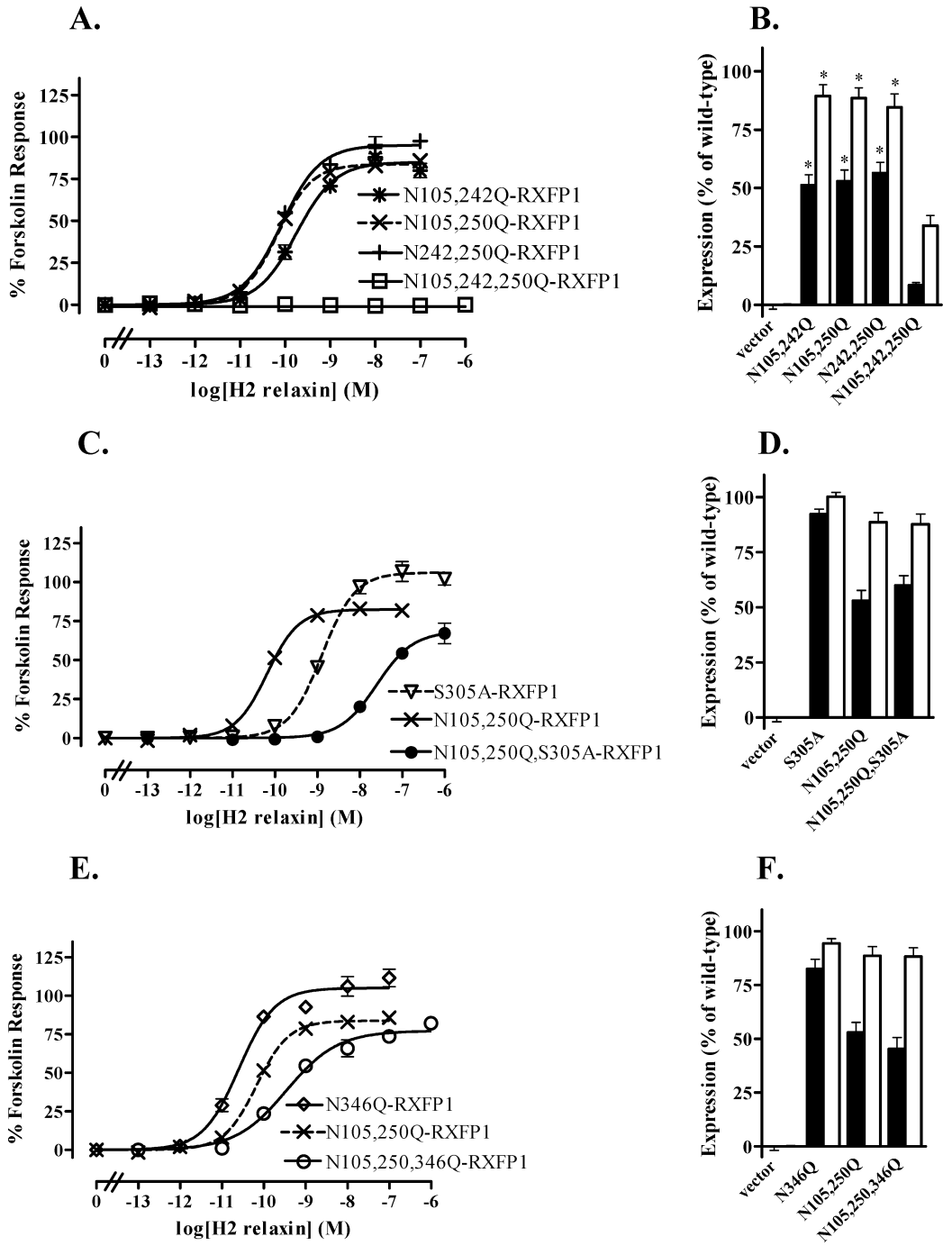

FIGURE 8: H2 relaxin-stimulated cAMP activity responses (A, C and E) and receptor expression (B, D, and F) of RXFP1 mutants at three glycosylation sites compared to the respective double site mutants: (A and B) N105,242,250Q-RXFP1 compared to N105,242Q-RXFP1, N105,250Q-RXFP1, and N242,250Q-RXFP1, (C and D) N105,250Q,S305A-RXFP1 compared to S305A-RXFP1 and N105,250Q-RXFP1, and (E and F) N105,250,346Q-RXFP1 compared to N346Q-RXFP1 and N105,250Q-RXFP1. cAMP activity is expressed as a percentage of the 5 μM forskolin response for each receptor. The amount of cell surface expression is determined by an ELISA using the anti-FLAG M1 monoclonal antibody to the FLAG epitope on whole cells. The amount of cell surface (black column) and total (white column) expression are presented as a percentage of the amount of wild-type RXFP1 expression with empty vector transfected HEK-293T cells being used to define 0%. Data are means $\pm$ the standard error of the mean from more than five experiments performed in triplicate. (*) $P < 0.001$ vs N105,242,250Q-RXFP1 (one-way ANOVA and Tukey's multiple-comparison test).

angiotensin receptor (*40*), there seem to be no detectable deficits in receptor function if N-glycosylation is ablated. For other receptors, such as V1a vasopressin receptor (*41*), impaired N-glycosylation is associated with a decreased level of cell surface expression of functional receptors. For other receptors, such as the secretin (*42*) and calcitonin receptors (*43*), deglycosyation causes a decrease in the level of ligand binding and potency of signaling but not cell surface expression. In our study, we have demonstrated that N-linked glycosylation of RXFP1 is necessary for both cell surface expression and receptor signaling but not primary ligand binding.

N-Linked glycosylation of RXFP1 is essential for intracellular trafficking of the receptor as shown by a significant reduction in both the maximum response of the cAMP assay and cell surface expression measured via an ELISA. N-Linked glycosylation at sites Asn-14 and Asn-105 individually has a minor influence on the cell surface delivery of the

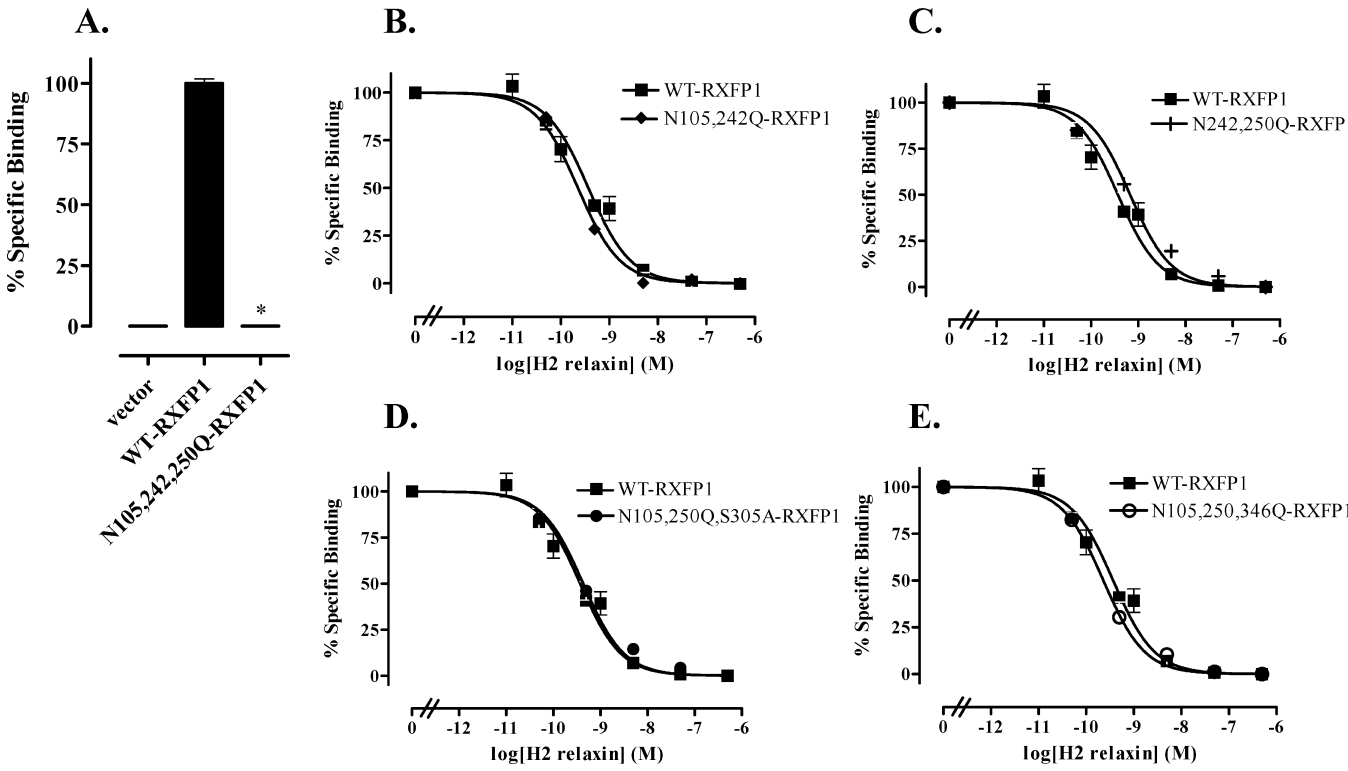

FIGURE 9: (A) Results of [^{33}P]H2 relaxin comparative binding at WT-RXFP1 compared to mutant N105,242,250Q-RXFP1. Specific [^{33}P]H2 relaxin binding is assessed in intact cells and is expressed as a percentage of the value for WT-RXFP1 (100%), with vector transfected cells used to define 0% binding. (*) $P < 0.001$ compared to WT-RXFP1 (one-way ANOVA and Tukey's multiple-comparison test). (B−E) Competition binding curves using [^{33}P]H2 relaxin comparing H2 relaxin binding affinities of multiple glycosylation site mutants to WT-RXFP1: (B) N105,242Q-RXFP1, (C) N242,250Q-RXFP1, (D) N105,250Q,S305A-RXFP1, and (E) N105,250,346Q-RXFP1. All data represent means ± the standard error of the mean of at least three individual experiments performed in triplicate.

receptor. We had previously demonstrated that N14Q-RXFP1 did not influence cell surface expression using an ELISA with the anti-FLAG monoclonal M2 antibody and a ^{125}I-labeled second antibody (*19*). However, in this study using the M1 monoclonal antibody and a fluorescently tagged second antibody, we were able to show that N14Q-RXFP1 exhibited a slightly reduced total level of expression and compromised cell surface expression compared to the wild-type receptor. Hence, the results of this study more closely mirror those of Kern et al. (*27*), who recently demonstrated that glycosylation at Asn-14 has a role in the regulation of intracellular trafficking of the receptor. Noticeably, when one or two of the other glycosylation mutants were combined with Asn-105, there was no further decrease in cell surface expression except with the triple mutant N105,242,250Q-RXFP1 which was not expressed at the cell surface at all. Importantly, the combination of ablation of Asn-242 and Asn-250 also resulted in a reduction in the level of cell surface expression. Hence, Asn-105, Asn-242, and Asn-250 are all essential for cell surface expression of RXFP1.

It is well recognized that N-linked oligosaccharides are necessary for the trafficking of receptors from the LGR family. Hence, FSHR, TSHR, and LHR all require some degree of N-linked glycosylation for optimal cell surface expression. FSHR contains three potential N-glycosylation sites, two of which are utilized in vitro (*44*). Mutation of both of these sites resulted in a nonfunctional receptor, while one intact site is sufficient for receptor expression at the cell surface and high-affinity ligand binding (*44*). The authors did not measure the level of cell surface expression in this whole cell study; however, they showed that removal of N-linked oligosaccharide from the mature receptor in detergent-solubilized extracts by extensive PNGase F digestion did not affect FSH binding (*44*), suggesting that indeed deglycosylation of both sites did abolish cell surface expression of the FSHR. This group also reported that removal of all six known N-glycosylation sites on the rat LHR had no effect on binding to human chorionic gonadotropin (*25*). More recently, results from another group suggest that the first three glycosylation sites in the rat LHR have a role in facilitating the processing of the receptor precursor to the mature cell surface form. Hence, deglycosylation resulted in defective processing of the precursor and therefore decreased the level of cell surface expression. These results show that the glycosylation of rat LHR plays an important role in LHR folding (*38*). Similarly, a series of human TSHR mutants with disruption of two of the six known N-glycosylation sites resulted in compromised cell surface expression of the receptors, without affecting TSH binding affinity and cAMP potency. Combinations of these sites with other single sites to create triple-glycosylation site mutants resulted in nonfunctional receptors. The authors did not assess cell surface expression; however, as the mutants did not bind TSH, they suggested that they may not fold correctly and may be trapped in the ER by the "quality control" system (*45*).

The importance of N-glycosylation in the trafficking of LGR family receptors to the cell surface is not surprising as N-glycosylation, which is added to the nascent receptor in the ER and is further processed in the Golgi apparatus, promotes folding not only directly by stabilizing nascent protein structure but also indirectly by serving as a recognition "tag" that allows glycoproteins to interact with a variety

of chaperones and glycosyltranferases. Some of these have a central role in folding and retention, while others target degradation (*46*). In the study presented here, the ablation of glycosylation in N105,242,250Q-RXFP1 not only resulted in lack of cell surface expression but also significantly reduced the total level of expression of the receptor, suggesting that disruption of glycosylation at those sites may cause misfolding and degradation of the receptor.

Ligand binding affinities for relaxin were determined using [^{33}P]H2 relaxin binding on whole cells. As we have shown previously (*19*), disruption of the glycosylation site in the LDLa module did not influence relaxin binding. Similarly, ablation of the LRR glycosylation sites at any single site or multiple sites did not change the affinity of the receptors for relaxin, suggesting that for RXFP1, N-glycosylation is not involved in ligand binding. Similarly, N-glycosylation does not influence ligand binding for the FSHR (*44*), LHR (*25, 38*), or TSHR (*45*).

This unchanged affinity for relaxin was reflected in an equivalent potency in relaxin-mediated cAMP signaling in all the single-site mutants except two: N14Q-RXFP1 and N303Q-RXFP1. Asn-14 is located in the LDLa module at the N-terminus of the receptor. Previously, we showed that N14Q-RXFP1 had a potency similar to that of WT-RXFP1; however, in this study, we showed a slight reduction in potency which is consistent with the observation from another study (*27*). In contrast to this small effect with Asn-14, ablation of Asn-303 resulted in a 100-fold lower potency in relaxin-stimulating cAMP activity. An additional mutant, S305A-RXFP1, was assessed to ensure that the more drastically weakened ability to stimulate cAMP shown in N303Q-RXFP1 was not simply associated with the mutation of asparagine 303 to glutamine. This mutant was shown to have a similar reduced potency. It is therefore likely that glycosylation at position 303 is necessary for optimal functioning of RXFP1.

Interestingly, although the other LRR glycosylation sites had no influence on cAMP signaling on their own, when they were combined to form double-glycosylation site mutants this led to decreased relaxin-stimulated cAMP potency, although this was only significant in two cases. However, when combined with a further site in the triple-site mutant N105,250,346Q-RXFP1, there was an almost 10-fold reduction in potency. Additionally, when S305A-RXFP1 was combined with two of these sites to construct N105, 250Q, S305A-RXFP1, there was also a 10-fold reduction in potency compared to that of the single-site mutation. Hence, although Asn-105, Asn-250, and Asn-346 do not play any part in receptor signaling on their own, they might function in concert with Asn-303 to facilitate optimal RXFP1 cAMP signaling.

From our homology model of the LRRs of RXFP1, the phylogenetically conserved Asn-303 is located in the β-strand of LRR IX and is exposed on the surface of the inner concave β-sheet (Figure 1A). The concave β-sheet is thought to provide a recognition surface where specific protein−protein interactions occur (*47*). The presence of a glycosylation site at the middle position in C-terminal LRRs occurs often in other excellular LRR-containing proteins, such as members of the Toll-like receptor family (*48–50*), a large class of proteins with LRRs (*51*). Even though glycosylation on the inner concave surface is not unique to RXFP1, this site is of interest due to its proximity to the relaxin binding site. Recently, residues from LRRs IV−VIII of RXFP1 were implicated in binding to relaxin's well-characterized receptor binding triad (Arg-B14, Arg-B17, and Ile-B20) located in its B chain (*16*). In this model interaction, Arg-B14 is chelated by two acidic residues in the β-strand of LRR VIII of RXFP1 (E277 and D279). Although Asn-303 is located in the adjacent β-strand of LRR IX (Figure 1B), removal of oligosaccharides at this site did not affect the binding affinity of relaxin for RXFP1. Instead, receptor signaling was impaired by this change. Studies into the receptor mechanics of RXFP1 have revealed that multiple interactions are required for proper signaling. Primary, high-affinity binding to the ectodomain is the first step in receptor activation; however, secondary interactions are required between relaxin and the transmembrane domains before signal transduction can occur (*12, 18*). Considering Asn-303's central location in the LRRs of RXFP1, adjacent to the relaxin binding site, it is not unreasonable to conclude that glycosylation at this site may be important for the transformation of RXFP1 into its active conformation once primary relaxin binding has occurred. The other glycosylation sites which are located at varied positions in the LRRs could then work together with the oligosaccharide linkage at Asn-303 to create a receptor conformation that allows the crucial secondary interactions between relaxin and the transmembrane domains to occur. Conversely, Asn-303 in combination with the other glycosylation sites may be directly involved in the interactions that confer signaling of RXFP1.

Our analysis of RXFP1 sequences from multiple mammalian species has revealed that the N-linked glycosylation sites in human RXFP1 are highly conserved across species. This conservation and the functional roles that these sites play in receptor function make it likely that these sites are glycosylated in all of these mammalian species in vivo. The lack of a specific antibody for RXFP1 to perform immunoprecipitation, and the low level of endogenous expression of the receptor, precluded the study of RXFP1 glycosylation in vivo in this study. However, studies on the FSHR have clearly demonstrated that the glycosylation status of the receptor when expressed in mammalian cells in vitro are reflected in studies on the native receptor in vivo (*52, 53*).

ACKNOWLEDGMENT

We thank Tania Ferraro and Sharon Layfield for technical assistance.

REFERENCES

1. Schwabe, C., and McDonald, J. K. (1977) Relaxin: A disulfide homolog of insulin. *Science 197*, 914–915.
2. Burazin, T. C., Bathgate, R. A., Macris, M., Layfield, S., Gundlach, A. L., and Tregear, G. W. (2002) Restricted, but abundant, expression of the novel rat gene-3 (R3) relaxin in the dorsal tegmental region of brain. *J. Neurochem. 82*, 1553–1557.
3. Bathgate, R. A. D., Hsueh, A. J., and Sherwood, O. D. (2006) Physiology and Molecular Biology of the Relaxin Peptide Family, in *Physiology of Reproduction* (Neill, J. D., Ed.) 3rd ed., pp 679−770, Elsevier, San Diego.
4. Masini, E., Bani, D., Bello, M. G., Bigazzi, M., Mannaioni, P. F., and Sacchi, T. B. (1997) Relaxin counteracts myocardial damage induced by ischemia-reperfusion in isolated guinea pig hearts: Evidence for an involvement of nitric oxide. *Endocrinology 138*, 4713–4720.
5. Novak, J., Danielson, L. A., Kerchner, L. J., Sherwood, O. D., Ramirez, R. J., Moalli, P. A., and Conrad, K. P. (2001) Relaxin is

essential for renal vasodilation during pregnancy in conscious rats. *J. Clin. Invest. 107*, 1469–1475.
6. Osheroff, P. L., and Phillips, H. S. (1991) Autoradiographic localization of relaxin binding sites in rat brain. *Proc. Natl. Acad. Sci. U.S.A. 88*, 6413–6417.
7. Ma, S., Roozendaal, B., Burazin, T. C., Tregear, G. W., McGaugh, J. L., and Gundlach, A. L. (2005) Relaxin receptor activation in the basolateral amygdala impairs memory consolidation. *Eur. J. Neurosci. 22*, 2117–2122.
8. Samuel, C. S., Du, X. J., Bathgate, R. A., and Summers, R. J. (2006) 'Relaxin' the stiffened heart and arteries: The therapeutic potential for relaxin in the treatment of cardiovascular disease. *Pharmacol. Ther. 112*, 529–552.
9. Seibold, J. R., Korn, J. H., Simms, R., Clements, P. J., Moreland, L. W., Mayes, M. D., Furst, D. E., Rothfield, N., Steen, V., Weisman, M., Collier, D., Wigley, F. M., Merkel, P. A., Csuka, M. E., Hsu, V., Rocco, S., Erikson, M., Hannigan, J., Harkonen, W. S., and Sanders, M. E. (2000) Recombinant human relaxin in the treatment of scleroderma. A randomized, double-blind, placebo-controlled trial. *Ann. Intern. Med. 132*, 871–879.
10. Hsu, S. Y., Nakabayashi, K., Nishi, S., Kumagai, J., Kudo, M., Sherwood, O. D., and Hsueh, A. J. (2002) Activation of orphan receptors by the hormone relaxin. *Science 295*, 671–674.
11. Bathgate, R. A., Ivell, R., Sanborn, B. M., Sherwood, O. D., and Summers, R. J. (2006) International Union of Pharmacology LVII: Recommendations for the nomenclature of receptors for relaxin family peptides. *Pharmacol. Rev. 58*, 7–31.
12. Sudo, S., Kumagai, J., Nishi, S., Layfield, S., Ferraro, T., Bathgate, R. A., and Hsueh, A. J. (2003) H3 relaxin is a specific ligand for LGR7 and activates the receptor by interacting with both the ectodomain and the exoloop 2. *J. Biol. Chem. 278*, 7855–7862.
13. Kumagai, J., Hsu, S. Y., Matsumi, H., Roh, J. S., Fu, P., Wade, J. D., Bathgate, R. A., and Hsueh, A. J. (2002) INSL3/Leydig insulin-like peptide activates the LGR8 receptor important in testis descent. *J. Biol. Chem. 277*, 31283–31286.
14. Hsu, S. Y. (2003) New insights into the evolution of the relaxin-LGR signaling system. *Trends Endocrinol. Metab. 14*, 303–309.
15. Vassart, G., Pardo, L., and Costagliola, S. (2004) A molecular dissection of the glycoprotein hormone receptors. *Trends Biochem. Sci. 29*, 119–126.
16. Bullesbach, E. E., and Schwabe, C. (2005) The trap-like relaxin-binding site of the leucine-rich G-protein-coupled receptor 7. *J. Biol. Chem. 280*, 14051–14056.
17. Scott, D. J., Wilkinson, T. N., Zhang, S., Ferraro, T., Wade, J. D., Tregear, G. W., and Bathgate, R. A. (2007) Defining the LGR8 residues involved in binding insulin-like peptide 3. *Mol. Endocrinol. 21*, 1699–1712.
18. Halls, M. L., Bond, C. P., Sudo, S., Kumagai, J., Ferraro, T., Layfield, S., Bathgate, R. A., and Summers, R. J. (2005) Multiple binding sites revealed by interaction of relaxin family peptides with native and chimeric relaxin family peptide receptors 1 and 2 (LGR7 and LGR8). *J. Pharmacol. Exp. Ther. 313*, 677–687.
19. Scott, D. J., Layfield, S., Yan, Y., Sudo, S., Hsueh, A. J., Tregear, G. W., and Bathgate, R. A. (2006) Characterization of novel splice variants of LGR7 and LGR8 reveals that receptor signaling is mediated by their unique low density lipoprotein class A modules. *J. Biol. Chem. 281*, 34942–34954.
20. Hopkins, E. J., Layfield, S., Ferraro, T., Bathgate, R. A., and Gooley, P. R. (2007) The NMR solution structure of the relaxin (RXFP1) receptor lipoprotein receptor class A module and identification of key residues in the N-terminal region of the module that mediate receptor activation. *J. Biol. Chem. 282*, 4172–4184.
21. Lanctot, P. M., Leclerc, P. C., Clement, M., Auger-Messier, M., Escher, E., Leduc, R., and Guillemette, G. (2005) Importance of N-glycosylation positioning for cell-surface expression, targeting, affinity and quality control of the human AT1 receptor. *Biochem. J. 390*, 367–376.
22. Fan, G., Goldsmith, P. K., Collins, R., Dunn, C. K., Krapcho, K. J., Rogers, K. V., and Spiegel, A. M. (1997) N-linked glycosylation of the human Ca^{2+} receptor is essential for its expression at the cell surface. *Endocrinology 138*, 1916–1922.
23. Michineau, S., Alhenc-Gelas, F., and Rajerison, R. M. (2006) Human bradykinin B2 receptor sialylation and N-glycosylation participate with disulfide bonding in surface receptor dimerization. *Biochemistry 45*, 2699–2707.
24. Kaushal, S., Ridge, K. D., and Khorana, H. G. (1994) Structure and function in rhodopsin: The role of asparagine-linked glycosylation. *Proc. Natl. Acad. Sci. U.S.A. 91*, 4024–4028.
25. Davis, D. P., Rozell, T. G., Liu, X., and Segaloff, D. L. (1997) The six N-linked carbohydrates of the lutropin/choriogonadotropin receptor are not absolutely required for correct folding, cell surface expression, hormone binding, or signal transduction. *Mol. Endocrinol. 11*, 550–562.
26. Yan, Y., Cai, J., Fu, P., Layfield, S., Ferraro, T., Kumagai, J., Sudo, S., Tang, J. G., Giannakis, E., Tregear, G. W., Wade, J. D., and Bathgate, R. A. (2005) Studies on soluble ectodomain proteins of relaxin (LGR7) and insulin 3 (LGR8) receptors. *Ann. N.Y. Acad. Sci. 1041*, 35–39.
27. Kern, A., Agoulnik, A. I., and Bryant-Greenwood, G. D. (2007) The low-density lipoprotein class A module of the relaxin receptor (leucine-rich repeat containing G-protein coupled receptor 7): Its role in signaling and trafficking to the cell membrane. *Endocrinology 148*, 1181–1194.
28. Altschul, S. F., Madden, T. L., Schaffer, A. A., Zhang, J., Zhang, Z., Miller, W., and Lipman, D. J. (1997) Gapped BLAST and PSI-BLAST: A new generation of protein database search programs. *Nucleic Acids Res. 25*, 3389–3402.
29. Thompson, J. D., Higgins, D. G., and Gibson, T. J. (1994) CLUSTAL W: Improving the sensitivity of progressive multiple sequence alignment through sequence weighting, position-specific gap penalties and weight matrix choice. *Nucleic Acids Res. 22*, 4673–4680.
30. Schwede, T., Kopp, J., Guex, N., and Peitsch, M. C. (2003) SWISS-MODEL: An automated protein homology-modeling server. *Nucleic Acids Res. 31*, 3381–3385.
31. Kaplan, W., and Littlejohn, T. G. (2001) Swiss-PDB Viewer (Deep View). *Brief Bioinf. 2*, 195–197.
32. Melo, F., and Feytmans, E. (1998) Assessing protein structures with a non-local atomic interaction energy. *J. Mol. Biol. 277*, 1141–1152.
33. Hooft, R. W., Vriend, G., Sander, C., and Abola, E. E. (1996) Errors in protein structures. *Nature 381*, 272.
34. Chen, W., Shields, T. S., Stork, P. J., and Cone, R. D. (1995) A colorimetric assay for measuring activation of Gs- and Gq-coupled signaling pathways. *Anal. Biochem. 226*, 349–354.
35. Kobe, B., and Kajava, A. V. (2001) The leucine-rich repeat as a protein recognition motif. *Curr. Opin. Struct. Biol. 11*, 725–732.
36. Barton, W. A., Liu, B. P., Tzvetkova, D., Jeffrey, P. D., Fournier, A. E., Sah, D., Cate, R., Strittmatter, S. M., and Nikolov, D. B. (2003) Structure and axon outgrowth inhibitor binding of the Nogo-66 receptor and related proteins. *EMBO J. 22*, 3291–3302.
37. Muda, M., He, C., Martini, P. G., Ferraro, T., Layfield, S., Taylor, D., Chevrier, C., Schweickhardt, R., Kelton, C., Ryan, P. L., and Bathgate, R. A. (2005) Splice variants of the relaxin and INSL3 receptors reveal unanticipated molecular complexity. *Mol. Hum. Reprod. 11*, 591–600.
38. Clouser, C. L., and Menon, K. M. (2005) N-linked glycosylation facilitates processing and cell surface expression of rat luteinizing hormone receptor. *Mol. Cell. Endocrinol. 235*, 11–19.
39. Ambasta, R. K., Ai, X., and Emerson, C. P., Jr. (2007) Quail Sulf1 function requires asparagine-linked glycosylation. *J. Biol. Chem. 282*, 34492–34499.
40. Servant, G., Dudley, D. T., Escher, E., and Guillemette, G. (1996) Analysis of the role of N-glycosylation in cell-surface expression and binding properties of angiotensin II type-2 receptor of rat pheochromocytoma cells. *Biochem. J. 313*, 297–304.
41. Hawtin, S. R., Davies, A. R., Matthews, G., and Wheatley, M. (2001) Identification of the glycosylation sites utilized on the V1a vasopressin receptor and assessment of their role in receptor signalling and expression. *Biochem. J. 357*, 73–81.
42. Ho, H. H., Gilbert, M. T., Nussenzveig, D. R., and Gershengorn, M. C. (1999) Glycosylation is important for binding to human calcitonin receptors. *Biochemistry 38*, 1866–1872.
43. Pang, R. T., Ng, S. S., Cheng, C. H., Holtmann, M. H., Miller, L. J., and Chow, B. K. (1999) Role of N-linked glycosylation on the function and expression of the human secretin receptor. *Endocrinology 140*, 5102–5111.
44. Davis, D., Liu, X., and Segaloff, D. L. (1995) Identification of the sites of N-linked glycosylation on the follicle-stimulating hormone (FSH) receptor and assessment of their role in FSH receptor function. *Mol. Endocrinol. 9*, 159–170.
45. Nagayama, Y., Nishihara, E., Namba, H., Yamashita, S., and Niwa, M. (2000) Identification of the sites of asparagine-linked glycosylation on the human thyrotropin receptor and studies on their role in receptor function and expression. *J. Pharmacol. Exp. Ther. 295*, 404–409.

46. Helenius, A., and Aebi, M. (2004) Roles of N-linked glycans in the endoplasmic reticulum. *Annu. Rev. Biochem. 73*, 1019–1049.
47. Kobe, B., and Deisenhofer, J. (1996) Mechanism of ribonuclease inhibition by ribonuclease inhibitor protein based on the crystal structure of its complex with ribonuclease A. *J. Mol. Biol. 264*, 1028–1043.
48. Choe, J., Kelker, M. S., and Wilson, I. A. (2005) Crystal structure of human toll-like receptor 3 (TLR3) ectodomain. *Science 309*, 581–585.
49. Weber, A. N., Morse, M. A., and Gay, N. J. (2004) Four N-linked glycosylation sites in human toll-like receptor 2 cooperate to direct efficient biosynthesis and secretion. *J. Biol. Chem. 279*, 34589–34594.
50. Sun, J., Duffy, K. E., Ranjith-Kumar, C. T., Xiong, J., Lamb, R. J., Santos, J., Masarapu, H., Cunningham, M., Holzenburg, A., Sarisky, R. T., Mbow, M. L., and Kao, C. (2006) Structural and functional analyses of the human Toll-like receptor 3. Role of glycosylation. *J. Biol. Chem. 281*, 11144–11151.
51. van der Hoorn, R. A., Wulff, B. B., Rivas, S., Durrant, M. C., van der Ploeg, A., de Wit, P. J., and Jones, J. D. (2005) Structure-function analysis of cf-9, a receptor-like protein with extracytoplasmic leucine-rich repeats. *Plant Cell 17*, 1000–1015.
52. Leifke, E., Simoni, M., Kamischke, A., Gromoll, J., Bergmann, M., and Nieschlag, E. (1997) Does the gonadotrophic axis play a role in the pathogenesis of Sertoli-cell-only syndrome? *Int. J. Androl. 20*, 29–36.
53. Gromoll, J., Simoni, M., Nordhoff, V., Behre, H. M., De Geyter, C., and Nieschlag, E. (1996) Functional and clinical consequences of mutations in the FSH receptor. *Mol. Cell. Endocrinol. 125*, 177–182.

BI800535B